INTERNATIONAL JOURNAL FOR NUMERICAL METHODS IN FLUIDS, VOL. 16, 725–738 (1993)

NUMERICAL SOLUTION OF THE GENERALIZED SERRE EQUATIONS WITH THE MACCORMACK FINITE-DIFFERENCE SCHEME

J. S. ANTUNES DO CARMO AND F. J. SEABRA SANTOS

Faculdade de Ciências e Tecnologia, Universidade de Coimbra, 3049 Coimbra Codex, Portugal

AND

A. B. ALMEIDA

Instituto Superior Técnico, Universidade Técnica de Lisboa, 1096 Lisboa Codex, Portugal

SUMMARY

This paper describes a two-dimensional numerical model to solve the generalized Serre equations. In order to solve the system of equations, written in the conservative form, we use an explicit finite-difference method based on the MacCormack time-splitting scheme. The numerical method and the computational model are validated by comparing one- and two-dimensional numerical solutions with theoretical and experimental results. Finally, the two-dimensional model (in a horizontal plane) is tested in a domain with complicated boundary conditions.

KEY WORDS Serre equations MacCormack's method Solitary waves Sudden releases

1. INTRODUCTION

The analysis of 1D and 2D unsteady flows by the Saint-Venant equations is very common. These equations can be solved by several implicit or explicit finite-element and finite-difference methods. Among the explicit methods, the MacCormack time-splitting scheme[1,2] has been used by a number of investigators.[3–8]

For the analysis of non-linear dispersive waves of Boussinesq equations (water waves with small relative amplitude propagating in shallow-water conditions), several finite-difference and finite-element methods have also been used.[9–13] However, these two types of equations do not reproduce with accuracy all kinds of waves in shallow-water conditions. In fact, the large-amplitude waves are well described by the Serre equations,[14] as can be seen in Seabra Santos.[15]

The numerical solutions of the Serre equations seem to be restricted, until now, to semi-implicit finite-difference schemes.[16–18]

The aim of this paper is to present a complete explicit finite-difference scheme in order to obtain the numerical solution of the generalized Serre equations (GSE).

2. FORMULATION

The generalized Serre equations (GSE) are deduced from the fundamental equations of fluid mechanics applied to a three-dimensional flow. Taking into account (1) the incompressibility of

0271–2091/93/080725–14$12.00

Received April 1992
Revised November 1992

the fluid; (2) the almost vertically uniform horizontal components of the velocity field (u, v), i.e.

$$u=\bar{u}(x, y, t)+u'(x, y, z, t) \quad \text{and} \quad v=\bar{v}(x, y, t)+v'(x, y, z, t),$$

with

$$\int u' \, dz=\int v' \, dz=0,$$

and considering the usual kinematic and dynamic conditions, the GSE equations are written in the conservative form, defining the dependent variables $Qx=h\,u$ and $Qy=h\,v$, as follows:[14]

$$\begin{gathered} h_t+(Qx)_x+(Qy)_y=0, \\ (Qx)_t+(u\,Qx)_x+(v\,Qx)_y+\{[(g+\beta)/2+\alpha/3]h^2\}_x=-(g+\beta+\alpha/2)h\,\xi_x-\tau x(\xi)+R\ \mathrm{div}(h\ \mathrm{grad}\ u), \\ (Qy)_t+(u\,Qy)_x+(v\,Qy)_y+\{[(g+\beta)/2+\alpha/3]h^2\}_y=-(g+\beta+\alpha/2)h\,\xi_y-\tau y(\xi)+R\ \mathrm{div}(h\ \mathrm{grad}\ v), \end{gathered} \tag{1}$$

where $\alpha=d^2h/dt^2$; $\beta=d^2\xi/dt^2$, and with the axis and the symbology presented in Figure 1.

The bottom friction terms, $\tau x(\xi)$ and $\tau y(\xi)$, are approximated by the classical steady-state Manning–Strickler formula, also written in terms of conservation variables as follows:

$$\tau x(\xi)=g\frac{Qx\sqrt{[(Qx)^2+(Qy)^2]}}{k^2\,h^{7/3}} \quad \text{and} \quad \tau y(\xi)=g\frac{Qy\sqrt{[(Qx)^2+(Qy)^2]}}{k^2\,h^{7/3}}.$$

The system of equations (1) constitutes, in accordance with the accepted assumptions, an adequate model for the study of high-amplitude waves propagating in shallow water. If the effect of the vertical acceleration of the fluid particles is neglected ($\alpha=\beta=0$), we obtain the classical Saint-Venant equations.[19]

3. NUMERICAL METHOD

Garcia and Kahawita,[3] solved the Saint-Venant equations using an explicit finite-difference method based on the MacCormack time-splitting scheme. In a similar way, in order to apply this method, the GSE (1) are 'split' into two systems of three equations throughout the Ox and Oy directions. The corresponding operators, Lx and Ly, take the following form:

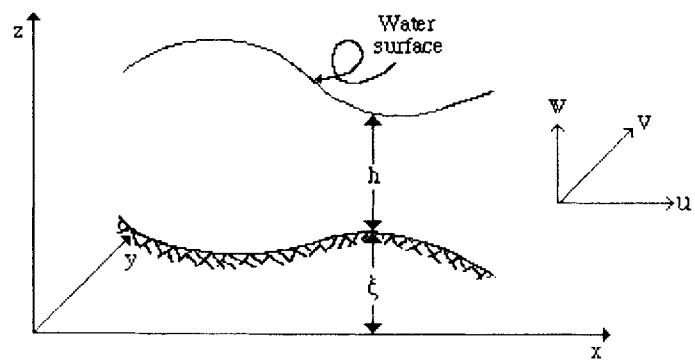

Figure 1. Notations

Operator Lx

$$h_t+(Qx)_x=0,$$

$$(Qx)_t+(u\,Qx)_x+\left[\left(\frac{g+\beta}{2}+\frac{\alpha}{3}\right)h^2\right]_x=-\left(g+\beta+\frac{\alpha}{2}\right)h\,\xi_x-\tau x(\xi)+R(Qx)_{xx}, \tag{2}$$

$$(Qy)_t+(u\,Qy)_x=R(Qy)_{xx}.$$

Operator Ly

$$h_t+(Qy)_y=0,$$

$$(Qx)_t+(v\,Qx)_y=R(Qx)_{yy}. \tag{3}$$

$$(Qy)_t+(v\,Qy)_y+\left[\left(\frac{g+\beta}{2}+\frac{\alpha}{3}\right)h^2\right]_y=-\left(g+\beta+\frac{\alpha}{2}\right)h\,\xi_y-\tau y(\xi)+R(Qy)_{yy},$$

Considering the generic variable F, the solution at time $(n+1)\,\Delta t$, for the computational point (i,j), is obtained from the known solution $F^n_{i,j}$ through the following symmetric application:

$$F^{n+1}_{i,j}=Lx\left(\frac{\Delta t}{4}\right)Ly\left(\frac{\Delta t}{4}\right)Lx\left(\frac{\Delta t}{4}\right)Ly\left(\frac{\Delta t}{4}\right)Ly\left(\frac{\Delta t}{4}\right)Lx\left(\frac{\Delta t}{4}\right)Ly\left(\frac{\Delta t}{4}\right)Lx\left(\frac{\Delta t}{4}\right)F^n_{i,j}, \tag{4}$$

where each operator, Lx and Ly, is composed of a predictor–corrector sequence and n represents a generic time t.

In the above application (4) of eight predictor–corrector sequences, alternately backward and forward space differences are used, as recommended by MacCormack[2] and Garcia and Kahawita,[3] and which we found totally justified.

The derivative discretization may be performed as follows:

First Lx operator:	Predictor—backward differences Corrector—forward differences
First Ly operator:	Predictor—backward differences Corrector—forward differences
Second Lx operator:	Predictor—forward differences Corrector—backward differences
Second Ly operator:	Predictor—forward differences Corrector—backward differences
Third Ly operatror:	Predictor—backward differences Corrector—forward differences
Third Lx operator:	Predictor—backward differences Corrector—forward differences
Fourth Ly operator:	Predictor—forward differences Corrector—backward differences
Fourth Lx operator:	Predictor—forward differences Corrector—backward differences

This computation sequence permits removal of most of the directional bias of this scheme, as is emphasized by Fennema and Chaudhry[6] for the Saint-Venant equations.

The first operator Lx of the above application F may be written as follows:

Predictor sequence (backward differences)

$$H^{p}_{i,j}=H^{0}_{i,j}-\frac{\Delta t}{4\Delta x}[(Qx)^{0}_{i,j}-(Qx)^{0}_{i-1,j}],$$

$$(Qx)^{p}_{i,j}=(Qx)^{0}_{i,j}-\frac{\Delta t}{4\Delta x}(D^{0}_{i,j}-D^{0}_{i-1,j})-\frac{\Delta t}{4\Delta x}\left(\frac{G^{0}_{i-1,j}+G^{0}_{i,j}}{2}\right)(\xi_{i,j}-\xi_{i-1,j})$$

$$-\frac{\Delta t}{4}(\tau x)^{0}_{i,j}+\frac{\Delta t}{4(\Delta x)^{2}}R[(Qx)^{0}_{i-1,j}-2(Qx)^{0}_{i,j}+(Qx)^{0}_{i+1,j}], \tag{5}$$

$$(Qy)^{p}_{i,j}=(Qy)^{0}_{i,j}-\frac{\Delta t}{4\Delta x}(E^{0}_{i,j}-E^{0}_{i-1,j})+\frac{\Delta t}{4(\Delta x)^{2}}R[(Qy)^{0}_{i-1,j}-2(Qy)^{0}_{i,j}+(Qy)^{0}_{i+1,j}].$$

Corrector sequence (forward differences)

$$H^{c}_{i,j}=\frac{1}{2}\left\{H^{0}_{i,j}+H^{p}_{i,j}-\frac{\Delta t}{4\Delta x}[(Qx)^{p}_{i+1,j}-(Qx)^{p}_{i,j}]\right\},$$

$$(Qx)^{c}_{i,j}=\frac{1}{2}\left\{(Qx)^{0}_{i,j}+(Qx)^{p}_{i,j}-\frac{\Delta t}{4\Delta x}(D^{p}_{i+1,j}-D^{p}_{i,j})-\frac{\Delta t}{4\Delta x}\left(\frac{G^{p}_{i,j}+G^{p}_{i+1,j}}{2}\right)(\xi_{i+1,j}-\xi_{i,j})\right.$$

$$\left.-\frac{\Delta t}{4}(\tau x)^{p}_{i,j}+\frac{\Delta t}{4(\Delta x)^{2}}R[(Qx)^{p}_{i-1,j}-2(Qx)^{p}_{i,j}+(Qx)^{p}_{i+1,j}]\right\}, \tag{6}$$

$$(Qy)^{c}_{i,j}=\frac{1}{2}\left\{(Qy)^{0}_{i,j}+(Qy)^{p}_{i,j}-\frac{\Delta t}{4\Delta x}(E^{p}_{i+1,j}-E^{p}_{i,j})+\frac{\Delta t}{4(\Delta x)^{2}}R[(Qy)^{p}_{i-1,j}-2(Qy)^{p}_{i,j}+(Qy)^{p}_{i+1,j}]\right\},$$

with $D=u\,Qx+[(g+\beta)/2+\alpha/3]h^{2}$, $E=u\,Qy$, $G=(g+\beta+\alpha/2)h$ and $H=h$.

After each predictor and each corrector of the application F the values of the velocities (u, v) are updated and the values of the vertical accelerations, α and β, are recalculated.

For computation of the vertical accelerations, the following schemes are used:

$$\alpha^{n}=\left(\frac{\mathrm{d}^{2}h}{\mathrm{d}t^{2}}\right)^{n}=\frac{\dot{h}^{n+1/2}-\dot{h}_{2}^{n-1/2}}{\Delta t}, \tag{7}$$

$$\beta^{n}=\left(\frac{\mathrm{d}^{2}\xi}{\mathrm{d}t^{2}}\right)^{n}=\frac{\dot{\xi}^{n+1/2}-\dot{\xi}_{2}^{n-1/2}}{\Delta t},$$

with

$$\dot{h}^{n+1/2}=\left(\frac{\mathrm{d}h}{\mathrm{d}t}\right)^{n+1/2}=\frac{h^{n+1}-h_{2}^{n}}{\Delta t},$$

$$\dot{\xi}^{n+1/2}=\left(\frac{\mathrm{d}\xi}{\mathrm{d}t}\right)^{n+1/2}=\frac{\xi^{n+1}-\xi_{2}^{n}}{\Delta t}.$$

The intermediate variables h_{2}^{n}, ξ_{2}^{n}, $\dot{h}_{2}^{n-1/2}$ and $\dot{\xi}_{2}^{n-1/2}$ have the following expressions:

$$h_{2}^{n}=h^{n}-\Delta t\,u^{n+1/2}\,h_{x}^{n+1/2}-\Delta t\,v^{n+1/2}\,h_{y}^{n+1/2},$$

$$\xi_{2}^{n}=\xi^{n}-\Delta t\,u^{n+1/2}\,\xi_{x}^{n+1/2}-\Delta t\,v^{n+1/2}\,\xi_{y}^{n+1/2},$$

$$\dot{h}_2^{n-1/2} = \dot{h}^{n-1/2} - \Delta t\, u^n (\dot{h}^n)_x - \Delta t\, v^n (\dot{h}^n)_y,$$

$$\dot{\xi}_2^{n-1/2} = \dot{\xi}^{n-1/2} - \Delta t\, u^n (\dot{\xi}^n)_x - \Delta t\, v^n (\dot{\xi}^n)_y,$$

with

$$\dot{h}^{n-1/2} = \frac{h^n - h^{n-1}}{\Delta t} + u^{n-1/2}\, h_x^{n-1/2} + v^{n-1/2}\, h_y^{n-1/2},$$

$$\dot{\xi}^{n-1/2} = \frac{\xi^n - \xi^{n-1}}{\Delta t} + u^{n-1/2}\, \xi_x^{n-1/2} + v^{n-1/2}\, \xi_y^{n-1/2}.$$

These expressions are also 'split' throughout the Ox and Oy directions in order to apply a numerical procedure based on the MacCormack scheme.

As can be seen, substituting the intermediate variable expressions in the above numerical schemes, the α^n and β^n values are approximated by

$$\alpha^n = \frac{\dfrac{h^{n+1} - h^n}{\Delta t} - \dfrac{h^n - h^{n-1}}{\Delta t}}{\Delta t} + \frac{u^{n+1/2}\, \dot{h}^{n+1/2} - u^{n-1/2}\, \dot{h}^{n-1/2}}{\Delta t} + \frac{v^{n+1/2}\, \dot{h}^{n+1/2} - v^{n-1/2}\, \dot{h}^{n-1/2}}{\Delta t}$$
$$+ u^n (\dot{h}^n)_x + v^n (\dot{h}^n)_y,$$

$$\beta^n = \frac{\dfrac{\xi^{n+1} - \xi^n}{\Delta t} - \dfrac{\xi^n - \xi^{n-1}}{\Delta t}}{\Delta t} + \frac{u^{n+1/2}\, \dot{\xi}^{n+1/2} - u^{n-1/2}\, \dot{\xi}^{n-1/2}}{\Delta t} + \frac{v^{n+1/2}\, \dot{\xi}^{n+1/2} - v^{n-1/2}\, \dot{\xi}^{n-1/2}}{\Delta t}$$
$$+ u^n (\dot{\xi}^n)_x + v^n (\dot{\xi}^n)_y,$$

with

$$\dot{h}^n = (\dot{h}^{n-1/2} + \dot{h}^{n+1/2})/2,$$

$$\dot{\xi}^n = (\dot{\xi}^{n-1/2} + \dot{\xi}^{n+1/2})/2.$$

Finally, it is important to note that the required intermediate variables at times $(n+1)\Delta t$ are approximated from the last predictor or corrector sequence calculated values h, u and v.

4. BOUNDARY CONDITIONS

The MacCormack scheme is not able to compute all the variables values in the points located at the boundaries of the domain. This problem was solved with recourse to the characteristics method in the predictor sequence; in the corrector sequence the derivatives discretization was reversed, when needed.

If the vertical accelerations, α and β, and the diffusion term $R(Qx)_{xx}$ are ignored in (2), we obtain the well-known Saint-Venant equations:

$$h_t + h\, u_x + u\, h_x = 0,$$

$$u\, h_t + h\, u_t + (h\, u^2)_x + \left(\frac{g h^2}{2}\right)_x = -g\, h\, \xi_x - g\, h\, J,$$

which allows us to obtain,

$$\frac{dx}{dt}=u\pm\sqrt{(gh)},$$

$$du\pm\sqrt{(g/h)}\,dh+g(\xi_x+J)\,dt=0.$$

Integrating these equations, taking into account the symbology presented in Figure 2, we obtain the following equations for the characteristics lines:

$$\text{Characteristic } C^-\begin{cases} U_p=U_d+g\dfrac{H_p-H_d}{C_d}-\left(\dfrac{\tau_c}{H_c}+g\dfrac{\xi_b-\xi_c}{X_b-X_c}\right)\Delta t, \\ X_p-X_d=(U_d-C_d)\Delta t, \end{cases} \tag{10}$$

$$\text{Characteristic } C^+\begin{cases} U_p=U_e-g\dfrac{H_p-H_e}{C_e}-\left(\dfrac{\tau_c}{H_c}+g\dfrac{\xi_c-\xi_a}{X_c-X_a}\right)\Delta t, \\ X_p-X_e=(U_e+C_e)\,\Delta t, \end{cases} \tag{11}$$

The parameters U_d, U_e, C_d, C_e, H_d and H_e presented in equations (10) and (11) have the following expressions, obtained by linear interpolation:[20]

$$\begin{aligned} U_d&=\frac{U_c-\theta[U_c(g\,H_b)^{1/2}-U_b(g\,H_c)^{1/2}]}{1-\theta[U_c-U_b-(g\,H_c)^{1/2}+(g\,H_b)^{1/2}]}, \\ U_e&=\frac{U_c+\theta[U_a(g\,H_c)^{1/2}-U_c(g\,H_a)^{1/2}]}{1+\theta[U_c-U_a+(g\,H_c)^{1/2}-(g\,H_a)^{1/2}]}, \\ C_d&=\frac{(g\,H_c)^{1/2}+U_d\theta[(g\,H_c)^{1/2}-(g\,H_b)^{1/2}]}{1+\theta[(g\,H_c)^{1/2}-(g\,H_b)^{1/2}]}, \\ C_e&=\frac{-(g\,H_c)^{1/2}+U_e\theta[(g\,H_c)^{1/2}-(g\,H_a)^{1/2}]}{\theta[(g\,H_a)^{1/2}-(g\,H_c)^{1/2}]-1}, \\ H_d&=H_c+\theta(U_d-C_d)\,(H_c-H_b), \\ H_e&=H_c-\theta(H_c-H_a)\,(U_e+C_e), \end{aligned} \tag{12}$$

with $\theta=\Delta t/\Delta x$.

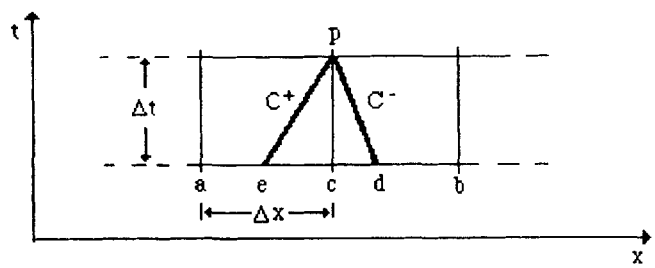

Figure 2. Local characteristic lines for subcritical flow

Equations (10) and (11) make it possible to compute explicitly the values of the flow depth h, at time $(n+1)\Delta t$, in the first and the last points of the mesh (when needed), respectively, along the Ox direction.

Similar computations are made, starting from the system of equations (3) along the Oy direction.

The radiation condition substitutes the conservation of momentum equations when backward differences are required for the first points of the mesh, or when forward differences are required for the last points of the mesh, throughout the Ox and Oy directions.

This condition takes the forms

$$\begin{aligned} &\pm(1-\gamma)\,\eta\, C\cos\varphi = h\,u \text{ along the } Ox \text{ direction},\\ &\pm(1-\gamma)\,\eta\, C\sin\varphi = h\,v \text{ along the } Oy \text{ direction}, \end{aligned} \tag{13}$$

where γ is a reflection coefficient; η is the surface elevation; $C=\sqrt{gh}$ is the wave celerity; φ is the angle which defines the direction of the wave propagation, related to the Ox direction.

We take the sign + or − according to the inflow or outflow boundary condition.

5. STABILITY CONDITIONS

The stability of an explicit finite-difference scheme is normally determined by the Courant–Friedrich–Lewy condition, that is,

$$\Delta t \le \max\left[\frac{Cr\,\Delta x}{(u+C)_{\max}}, \frac{Cr\,\Delta y}{(v+C)_{\max}}\right], \tag{14}$$

where Cr is the maximum Courant number that guarantees stable results. In the MacCormack scheme this is satisfied with $Cr=1$ for each set of operators.[1-3] However, comparisons of theoretical solutions with the one-dimensional results allow us to conclude that the global propagation Courant numbers of the proposed scheme must be under 3; moreover, the better global Courant number is of the order of 2. This means that the model presented can be used with Courant numbers between 0·50 and 0·75 for each set of operators.

The spatial discretization itself quite obviously has certain effects upon the quality of the solution. The better results were obtained with Δx and Δy in the same order of 0·9 $\bar{h}$ to $\bar{h}$, where $\bar{h}$ is the mean depth in the corresponding Δx or Δy interval.

6. COMPUTATIONAL TESTS

6.1. *Solitary waves*

In order to validate the proposed numerical method, some experiments were performed and compared with known analytical solutions.

Two of these experiments are shown in Figures 3 and 4. Both the cases represent a solitary wave travelling along a horizontal no-friction rectangular channel 2000 m long. The analytical solution of this problem is

$$\begin{aligned} h &= h_0 + \operatorname{sech}^2\left\{\left[\frac{3A}{4h_0^3(1+A/h_0)}\right]^{1/2}\left[x-\left[gh_0\left(1+\frac{A}{h_0}\right)\right]^{1/2}t+x_0\right]\right\},\\ u &= \left[gh_0\left(1+\frac{A}{h_0}\right)\right]^{1/2}\left(1-\frac{h_0}{h}\right), \end{aligned} \tag{15}$$

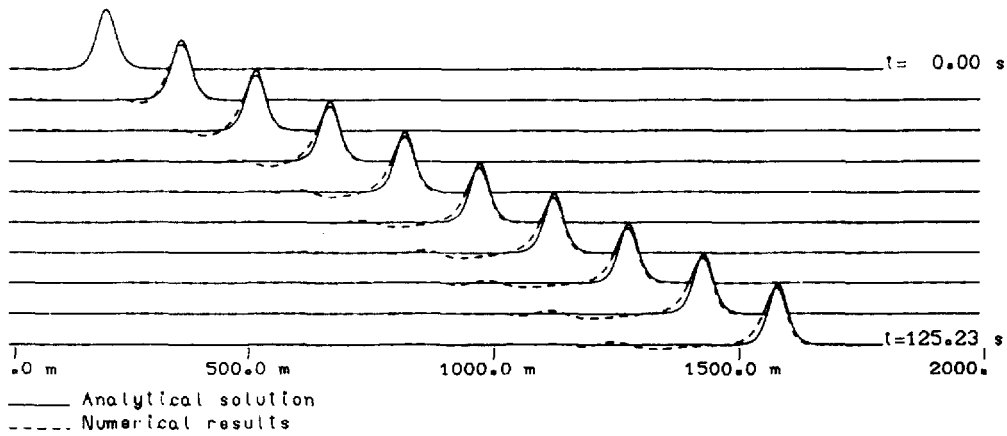

Figure 3. Propagation of a solitary wave with $A/h_0 = 0{\cdot}25$; $h_0 = 10$ m; horizontal bottom

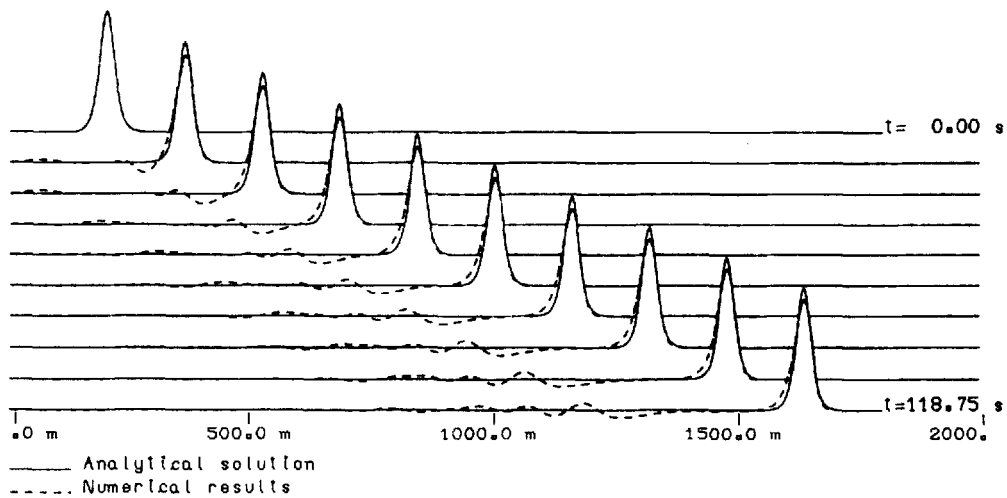

Figure 4. Propagation of a solitary wave with $A/h_0 = 0{\cdot}50$; $h_0 = 10$ m; horizontal bottom

where A is the wave amplitude, $h_0 = 10$ m is the undisturbed water depth for $t = 0$, and $x_0 = 200$ m is the initial position of the crest.

The results shown in Figure 3 are for a wave with $A/h_0 = 0{\cdot}25$, while Figure 4 shows the comparison with $A/h_0 = 0{\cdot}50$. Both experiments were computed with a spatial grid $\Delta x = 10$ m. The time increment Δt and the central processing unit (CPU) time required on a 8530 VAX computer were 1·74 s and 1·42 min for the first and 1·47 s and 1·49 min for the second experiment, respectively.

In both experiments the phase accuracy is very good; the amplitude of the wave decays of about 6–8% and the resulting loss of energy is responsible for the generation of a small numerical dispersive wave.

6.2. Sudden releases (dam-break experiments)

A set of data measurements is available, developed in the Hydraulic Laboratory of the Department of Civil Engineering of the University of Coimbra, for comparative analyses of the numerical scheme. A 7·50 m long by 0·30 m wide horizontal rectangular channel was used, with the dam located in the middle of the channel ($x = 3{\cdot}85$ m). The dam failed 'instantaneously' (in our experiments it is simulated by a glass sluice gate, which is operated by compressed air and opened in a very short time, about half a second). Four depth gauges were used, located at 2·65, 5·25, 6·25 and 7·25 m from the initial section of the channel, respectively.

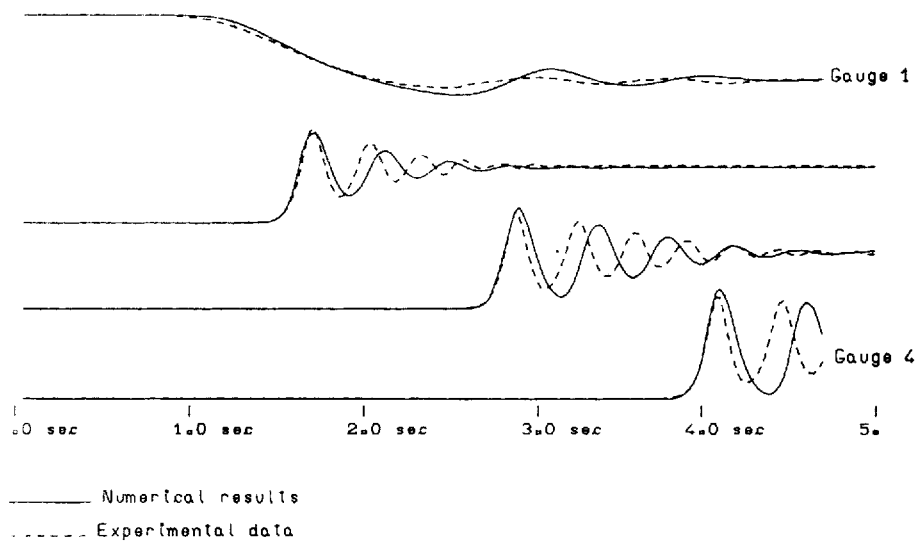

Figure 5. Sudden releases: ratio of the channel water-to-reservoir, $h_c/h_r = 0{\cdot}587$

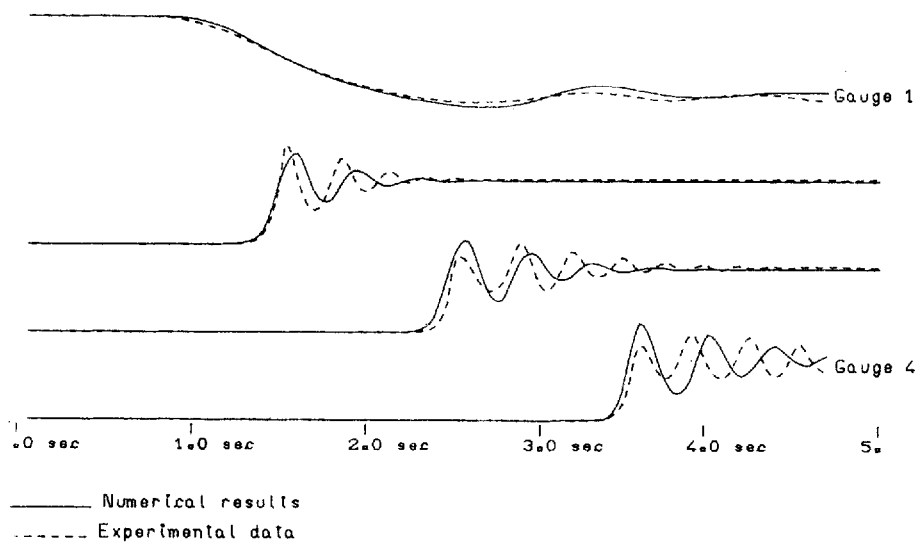

Figure 6. Sudden releases: ratio of the channel water-to-reservoir, $h_c/h_r = 0{\cdot}515$

Flow conditions were analysed for different ratios of the tailwater-to-reservoir depths (h_c/h_r). Only results for the ratios $h_c/h_r = 0{\cdot}587$ (Figure 5) and $h_c/h_r = 0{\cdot}515$ (Figure 6) are included here.

Figure 5 shows results for the numerical amplitude and phase accuracy of the first wave very close to the experimental data. Despite important remaining waves out of phase, the corresponding amplitudes agreed reasonably with the experimental data.

It is important to emphasize that the results shown in Figure 6 were obtained with the initial conditions $h_c = 0{\cdot}051$ m and $h_r = 0{\cdot}099$ m. This means that the ratio of maximum amplitude to water depth $\varepsilon = A/h_c \approx 0{\cdot}94$ exceeds the stability limits of the solitary wave; however, even in this case, the numerical amplitudes of the waves are in good accordance with the experimental data, excluding the first wave, which breaks.

These results were obtained with a $\Delta x = 0{\cdot}044$ m spacing grid and a time increment $\Delta t = 0{\cdot}083$ s for the first experiment; the results shown in Figure 6 were obtained with $\Delta x = 0{\cdot}050$ m and $\Delta t = 0{\cdot}10$ s.

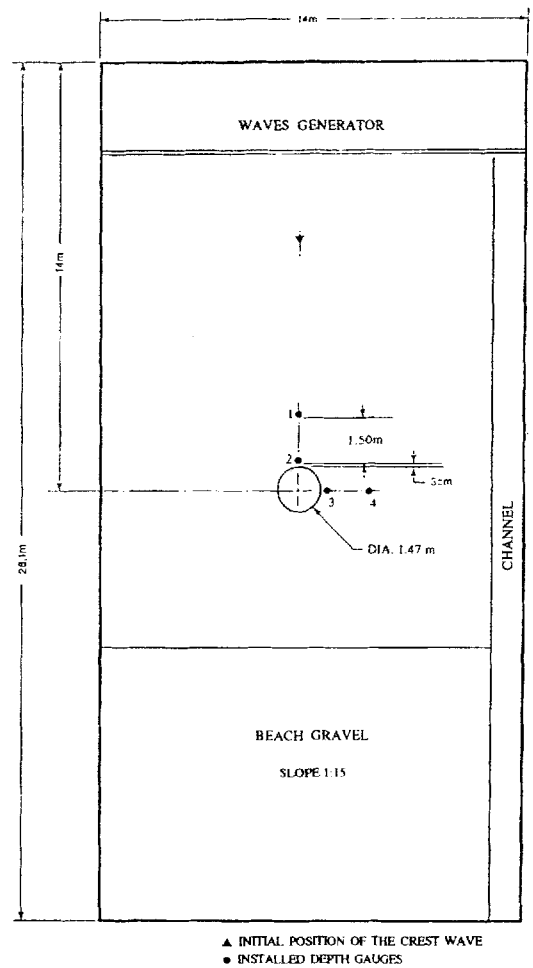

Figure 7. Physical model plan and installed depth gauges for a solitary wave overpassing an island

6.3. *Solitary wave overpassing an island*

The third application relates to a solitary wave propagation overpassing an island, whose boundaries are assumed to be vertical and totally reflective.

Figure 7 shows the physical model plan, including the positions of the installed depth gauges, conceived and realized by Temperville and Mansard.[21]

Figure 8 shows four surfaces of water computed at times $t_1 = 2{\cdot}35$ s, $t_2 = 4{\cdot}70$ s, $t_3 = 7{\cdot}05$ s and $t_4 = 9{\cdot}40$ s, and some comparisons between the numerical and experimental results are shown in Figure 9.

6.4. *Port of Figueira da Foz*

In order to test this model in a concrete case, the agitation established from a state of rest was calculated under a sinusoidal wave boundary condition, namely, with a period $T = 17{\cdot}5$ s, wave length $L = 173$ m, amplitude $A = 4{\cdot}70$ m in the open sea and direction $\Phi = 260°$ W.

The port of Figueira da Foz is protected by means of two roughed breakwaters, which are bordering greatly the outer harbour; a channel bordered almost exclusively by smooth inclined walls establish the liaison into the inner port, where the commercial quay is situated (Figure 10).

The port is 2250 m long and 400 m wide, approximately. Its average depth is of the order of 7 m, with approximately 12 m throughout the outer port basin.

The domain was modelled using an irregular spacing rectangular grid, with about 27 000 discrete points.

Figure 11 shows a perspective view of the surface computed in the basin 301 s after excitation.

As can be seen, a zone with stronger agitation is observed, under these conditions, in the centre of the outer harbour.

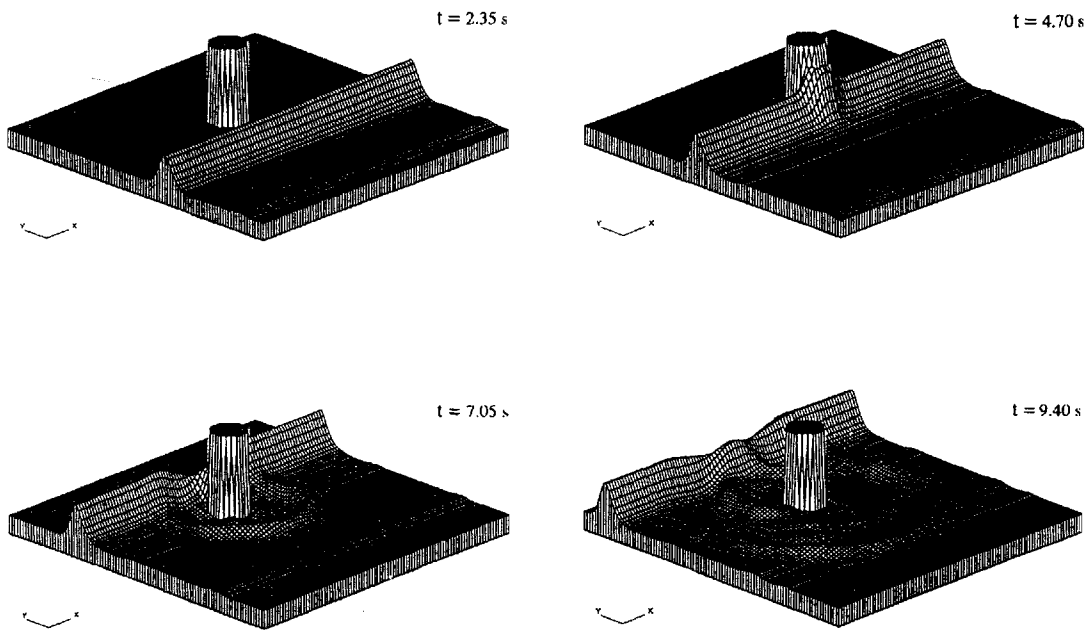

Figure 8. Three-dimensional perspective view of free-surface elevation for a solitary wave overpassing an island, in time sequence

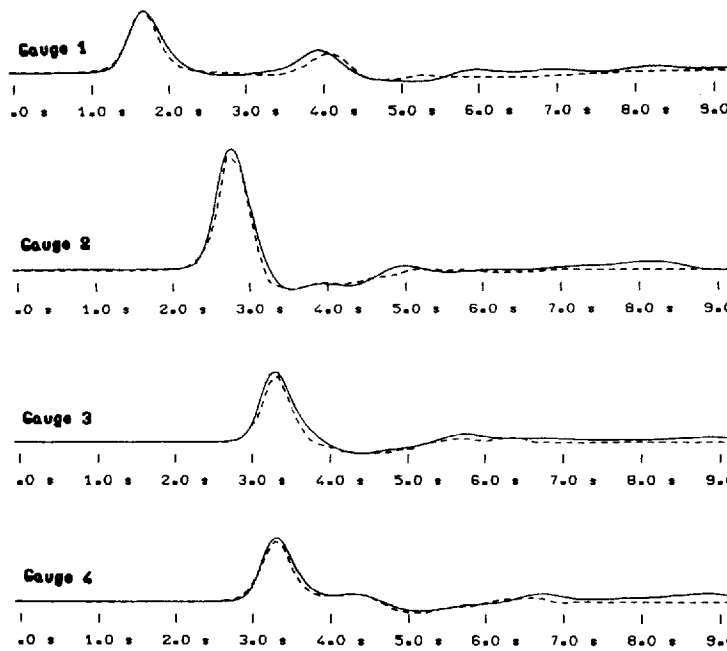

Figure 9. Comparison between numerical and experimental results for a solitary wave overpassing an island

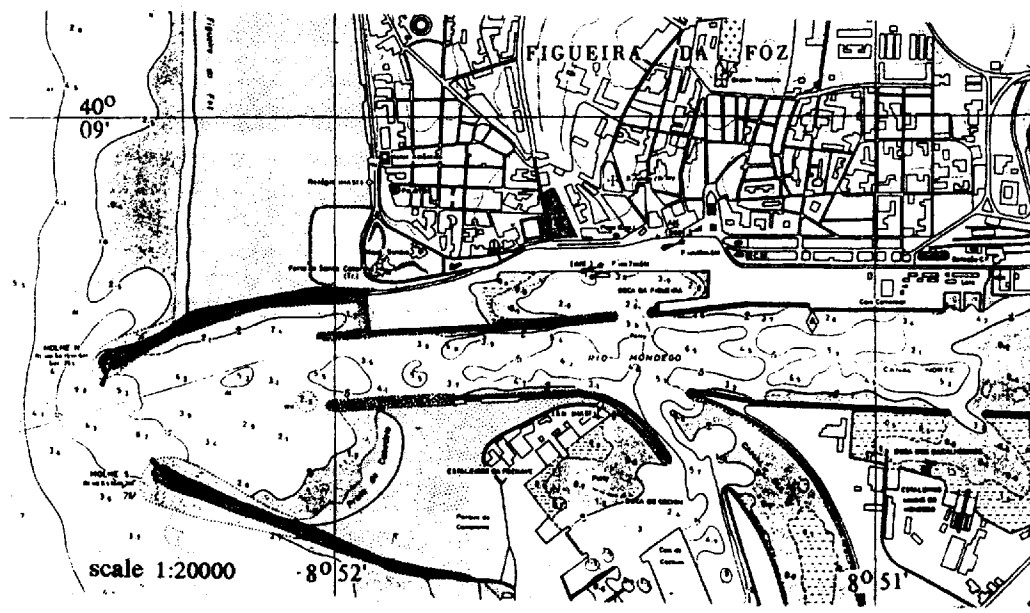

Figure 10. Base map of the port of Figueira da Foz

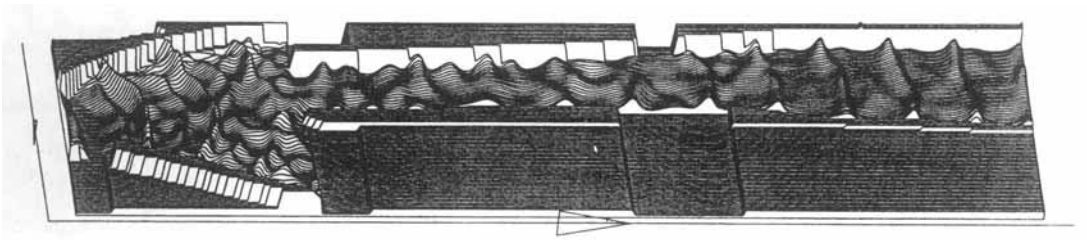

Figure 11. Port of Figueira da Foz. Perspective view of the surface computed 301 s after excitation

It is important to remark that this figure is the final result after adjusting the reflection coefficients in the breakwaters and channel walls in order to obtain in the port basin the agitation quite comparable to that observed under the same conditions.

7. CONCLUSIONS

A full explicit finite-difference method based on the MacCormack time-splitting scheme is developed in order to solve the generalized Serre equations.

Solitary waves of two amplitudes are propagated and compared with the analytical solution.

Dam-break experiments, with ratios $h_c/h_r \geq 0{\cdot}515$, are simulated and compared with laboratory-scale results.

In order to show the performances of the developed model in three-dimensional 'real-world' problems, two experiments are presented. The first consisted of a solitary wave overpassing an island and the second experiment is a concrete investigated case concerning the simulation of the agitation in the port of Figueira da Foz—Portugal.

The results obtained allow us to conclude that the model can be employed in any geometry, under complicated boundary conditions.

ACKNOWLEDGEMENTS

The authors express their appreciation to J. Lopes de Almeida (FCTUC) for the bathymetric data used in Figure 11 and his collaboration in generating three-dimensional perspective views.

REFERENCES

1. R. W. MacCormack, 'The effect of viscosity in hypervelocity impact cratering', *Paper 69-354*, American Institute of Aeronautics and Astronautics, Cincinnati, Ohio, 1969.
2. R. W. MacCormack, 'Numerical solution of the interaction of a shock wave with a laminar boundary layer', *Lecture Notes in Physics*, Vol. 8, Springer, Berlin 1971, pp. 151–163.
3. R. Garcia and R. A. Kahawita, 'Numerical solution of the Saint-Venant equations with the MacCormack finite-difference scheme', *Int. j. numer. methods fluids*, **6**, 259–274 (1986).
4. C. V. Bellos and J. G. Sakkas, '1D dam-break flood-wave propagation on dry bed', *J. Hydraul. Eng.*, **113**, 1510–1524 (1987).
5. R. J. Fennema and M. H. Chaudhry, 'Explicit numerical schemes for unsteady free-surface flows with shocks', *Water Resources Res.*, **22**, 1923–1930 (1986).
6. R. J. Fennema and M. H. Chaudhry, 'Explicit methods for 2D transient free-surface flows', *J. Hydraul. Eng.*, **116**, 1013–1034 (1990).
7. A. B. Franco, 'Simulação numérica de cheias provocadas por roturas de barragens', Tese de Mestrado em Hidráulica e Recursos Hídricos do IST, Lisboa, Portugal, 1989.
8. J. S. Antunes do Carmo, 'Efeitos hidrodinâmicos resultantes de deslizamentos de encostas em albufeiras—Modelação a duas dimensões horizontais', Tese de Mestrado em Hidraúlica e Recursos Hídricos do IST, Lisboa, Portugal, 1990.

9. D. H. Peregrine, 'Calculations of the development of an undular bore', *J. Fluid Mech.*, **25,** 321–330 (1966).
10. D. H. Peregrine, 'Long waves on a beach', *J. Fluid Mech.*, **27,** 815–827 (1967).
11. G. Pedersen and B. Gjevik, 'Run-up of solitary waves', *J. Fluid Mech.*, **135,** 183–299 (1983).
12. N. D. Katopodes and Chien-Tay Wu, 'Computation of finite-amplitude dispersive waves', *J. Waterway, Port, Coastal and Ocean Eng.*, **113,** 327–346 (1987).
13. D. R. Basco, 'Limitations of the Saint-Venant equations in dam-break analysis', *J. Hydraul. Eng.*, **115,** 950–965 (1989).
14. F. Serre, 'Contribution à l'étude des écoulements permanents et variables dans les canaux', La Houille Blanche, 1953, pp. 374–388.
15. F. J. Seabra Santos, D. P. Renouard and A. M. Temperville, 'Etude théorique et expérimentale des domaines de validité des théories d'évolution des ondes en eau peu profonde', *Annales Geophysicae*, **6,** 671–680 (1988).
16. A. Hauguel, 'Calcul des houles de tempêtes en eau peu profonde; application à l'agitation dans les ports', Rapport interne EDF—Chatou, France, 1979.
17. J. P. Benqué, A. Hauguel and P. L. Viollet, *Engineering Applications of Computational Hydraulics*, Vol. II, Pitman, London, 1982.
18. F. J. Seabra Santos, 'Contribution a l'étude des ondes de gravité bidimensionnelles en eau peu profonde', Université Scientifique et Médicale et Institut National Polytechnique de Grenoble-France, 1985.
19. Saint-Venant, *C.R. Acad. Sci.*, **83,** 147, 237 (1871).
20. A. B. Almeida, 'Introdução ao estudo dos escoamentos variáveis em superfície livre (modelação matemática)', IST, Lisboa, Portugal, 1983.
21. A. Temperville and E. Mansard, *Internal Report*, CNRC Ottawa, Canada, 1988.